Bull. Mater. Sci., Vol. 18, No. 8, December 1995, pp. 963–974. © Printed in India.

Synthesis of high-energy-density $Pr_2Fe_{14-x}Co_xB$, $x \leqslant 3$, magnets for practical applications†

S HALDAR, S RAM*, P RAMACHANDRARAO and H D BANERJEE**
National Metallurgical Laboratory, Jamshedpur 831 007, India
*Present Address: Institute of Metal Research, T.U. Berlin, Hardenbergstraße-36, D-10623, Berlin, Germany
** Materials Science Centre, Indian Institute of Technology, Kharagpur 721 302, India

Abstract. Stable magnetic powders, of 1–2 μm particle size, of partially Co-substituted, $Pr_2Fe_{14-x}Co_xB$, $x \leqslant 3$, alloys together with 2–4 at% excess Pr were prepared by rapidly quenching the associated melts into thin ribbons and then mechanical attriting the ribbons in the refined particle sizes. The saturation magnetization M_s, remanent magnetization J_r, intrinsic coercivity H_{ci} and Curie temperature T_c were studied in characterizing the powders for fabricating into sintered or polymer bonded magnets. It is found that the small $x = 0{\cdot}4$ 0·8 substitution of the Co on Fe sites in this series sensitively leads to an increase in the value of H_{ci}, by as much as 40%, with the optimum value of 21 kOe at $x \sim 0{\cdot}55$, together with an improvement in the T_c from 292°C to 325°C, without significantly diluting the $M_s \sim 150$ emu/g and $J_r \sim 8{\cdot}0$ kG values. The Co-substituted $Pr_2Fe_{14}B$ alloy particles are better stable and corrosion resistant in ambient atmosphere. The results are discussed with the microstructure and comparison with the data for $Nd_2Fe_{14}B$ powders processed under the same conditions.

Keywords. Stable magnetic powders; $Pr_2Fe_{14-x}Co_xB$.

1. Introduction

Since the discovery of $P4_2/mnm$ tetragonal $Nd_2Fe_{14}B$ phase as an excellent high-energy-density magnetic material (Herbst *et al* 1984; Buschow 1986), much research has been devoted to improve its stability with stable magnetic properties using different substitutions by different methods (Buschow 1986; Deruelle *et al* 1990; Lim *et al* 1991; Ram and Joubert 1992; Ram 1994, 1995; Ram *et al* 1995). 5–10 wt% excess rare-earth (R) in the $R_2Fe_{14}B$ series thus promptly stabilizes the hard magnetic phase with desired magnetic properties. It supports the high coercivity of the product and protects it against oxidation corrosion in ambient atmosphere, but adversely dilutes the total magnetic moment.

A high quality permanent magnet for high power dc motors, electricity generators, and other similar applications usually require a symmetric hysteresis loop with constant (and as high as possible) values of the saturation magnetization M_s, remanent magnetization J_r (or B_r) and/or coercivity H_c, which in turn result in a high value of the energy-product $(BH)_{max}$, over a wide range of temperature of operation. In this respect, amongst the whole rare-earth $R_2Fe_{14}B$ series, the Nd and Pr based magnets are most widely applied. The intrinsic magnetic properties, i.e. the saturation magnetization M_s, magnetocrystalline anisotropy H_a (or the anisotropy constants K_1 and K_2), or the Curie temperature T_c, of $Pr_2Fe_{14}B$ are very similar to those of $Nd_2Fe_{14}B$ (Buschow 1986). However, the neodymium is the most abundant and therefore the Nd–Fe–B alloys are less expensive and commercially easily available.

†Paper presented at the poster session of MRSI AGM VI, Kharagpur, 1995

A disadvantage with the $Nd_2Fe_{14}B$ is that it is not uniaxial throughout its ferromagnetic range. Magnetic moments of the Nd and Fe atoms in the tetragonal $Nd_2Fe_{14}B$ crystal lattice are collinear with the easy axis of the magnetization (that is along the crystallographic c-axis) only over limited $T \geqslant T_{SR}$ temperatures, and undergo spin-reorientation transitions at T_{SR}, called the spin-reorientation transition temperature, distorting the hysteresis loop at lower temperatures (Givord *et al* 1986; Nishio *et al* 1990). This is ruled out in $Pr_2Fe_{14}B$, in which the Pr and Fe magnetic spins remain collinear along the c-axis up to 0 K. This is discussed with the synthesis of stable $Pr_{2+\delta}Fe_{14}B$ powders, using a small 3–16 at% substitution of Co on the Fe sites together with an excess ($\delta \sim 0{\cdot}538$) Pr, with superior magnetic properties for practical applications as permanent magnets and other devices, in this article.

2. Experimental

The two series of polycrystalline alloys $Pr_2Fe_{14-x}Co_xB$($x \leqslant 3{\cdot}0$) and $Nd_2Fe_{14-x}Co_xB$ ($x \leqslant 3{\cdot}0$) were prepared by melting 99·9% pure ingots of the constituent elements at $\sim$ 1200°C in a boron nitride crucible by induction melting. Since the rare-earths Pr and Nd are somewhat volatile at this temperature, we started the reaction with 10–20% excess amounts of them over the $R_2Fe_{14}B$ phase. The boron content was maintained at stoichiometric level $\sim$ 6 at% and the iron (cobalt) accounted for the balance. The recovered alloys were pulverized by a jaw crusher and a pin mill in an Ar atmosphere. 15–30 μm thin ribbons were melt-spun by ejecting the molten alloy on the surface of a rapidly spinning copper wheel under a pure Ar gas. Finally, the ribbons were cut, crushed and milled in fine powders of 1–2 μm particle size, as discussed earlier (Ram 1995).

X-ray diffractogram, recorded using filtered Co–Kαl radiation ($\lambda = 0{\cdot}17903$ nm) on a Siemens Kristalloflex X-ray diffractometer, was used to characterize the formation of the primary ferromagnetic $R_2Fe_{14}B$ phase in the melt spun ribbons subsequent to thermal annealing between 500–700°C, if necessary. The microstructures were studied with a JEOL 35 CF scanning electron microscope equipped with an X-ray detector for compositional analysis. Compositional maps of the primary phase showed Fe/Pr (or Nd) ratio varying between 6·8 and 7·5, which is very close to the ratio 14·2 in the $R_2Fe_{14}B$ structure.

The magnetic properties, i.e. the saturation magnetization (M_s), remanent magnetization (J_r) and intrinsic coercivity (H_{ci}), were measured using a vibrating sample magnetometer or a hysteresisgraph. The Curie temperature (T_c) was determined from thermomagnetogram, which was measured by heating the specimen (by a heating rate of 10°C/min) between 25 and 600°C, at a magnetic field of 1–2 kOe, with a similar magnetometer in conjunction with a high temperature oven assembly to control and vary the temperature.

3. Results and discussion

3.1 *Microstructure, electron microprobe analysis and magnetic properties*

Scanning electron micrographs of the polycrystalline R–Fe–B samples exhibit platelet shaped particles of the ferromagnetic $R_2Fe_{14}B$ phase, with R for Pr or Nd. In the

Figure 1. Scanning electron micrograph of a refined Pr–Fe–B powder of 1–2 μm particle size. The scale bar refers to 2 μm.

Table 1. Magnetic properties of typical hot-pressed R–Fe–B alloys.

Composition	M_s (emu/g)	H_{ci} (kOe)	J_r (kG)	T_c (°C)
$Nd_{12}Fe_{82}B_6$	165	5	8·5	315
$Nd_{14\cdot5}Fe_{80}B_{5\cdot5}$	163	25	7·5	—
$Pr_{14\cdot5}Fe_{80}B_{5\cdot5}$	155	15	7·2	292
$Nd_{14\cdot5}Fe_{75}Co_5B_{5\cdot5}$	158	16	8·2	350
$Pr_{14\cdot5}Fe_{75}Co_5B_{5\cdot5}$	153	18	8·0	—
$Pr_{14\cdot5}Fe_{76\cdot9}Co_{3\cdot1}B_{5\cdot5}$	154	21	8·1	—
$Pr_{15\cdot5}Fe_{63}Co_{16}B_{5\cdot5}$	150	17	7·8	429

crystallized melt-spun ribbons, the particle size varies over a wide range between 1 and 50 μm, but those of milled in refined powder present a reasonably sharp size distribution in the range, 1–2 μm. For example, figure 1 shows a typical micrograph of a typical Pr–Fe–B alloy of final composition of $Pr_{14\cdot5}Fe_{80}B_{5\cdot5}$ (or $Pr_{2+\delta}Fe_{14}B$, with $\delta = 0{\cdot}538$), as analysed by the electron microprobe analysis. The final compositions of all the alloys studied here are summarized in table 1.

The saturation magnetization M_s, intrinsic coercivity H_{ci}, remanent magnetization J_r, and Curie temperature T_c of the samples are included in table 1. It is interesting to learn that small Co-substitutions ($x \leqslant 3$) in the $Pr_{2+\delta}Fe_{14-x}Co_xB$ series, having the $\delta = 0{\cdot}538$ excess Pr, very sensitively leads to considerable improvement in the H_{ci} value (figure 2). For example, $x = 0{\cdot}2$–$0{\cdot}8$ cobalt improves the H_{ci} by as much as 40% without significantly diluting the $M_s \sim 150$ emu/g or $J_r \sim 8{\cdot}0$ kG (figure 3) value. An optimum value of $H_{ci} = 21$ kOe (with $J_r = 8{\cdot}1$ kG) was thus found for the optimal composition of $x \sim 0{\cdot}55$ at room temperature. The high H_{ci} value monotonically drops to the original Co free value at $x \sim 1{\cdot}5$ and then almost linearly decreases as a function of x, basically governed

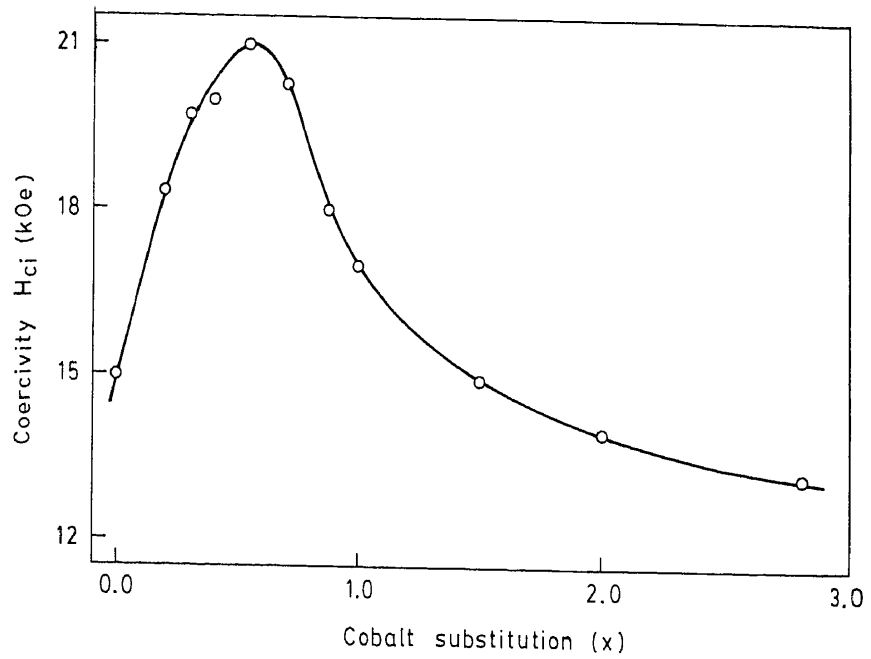

Figure 2. Effect of the cobalt substitution (x) on coercivity H_{ci} in $Pr_{2+\delta}Fe_{14-x}Co_xB$ powders.

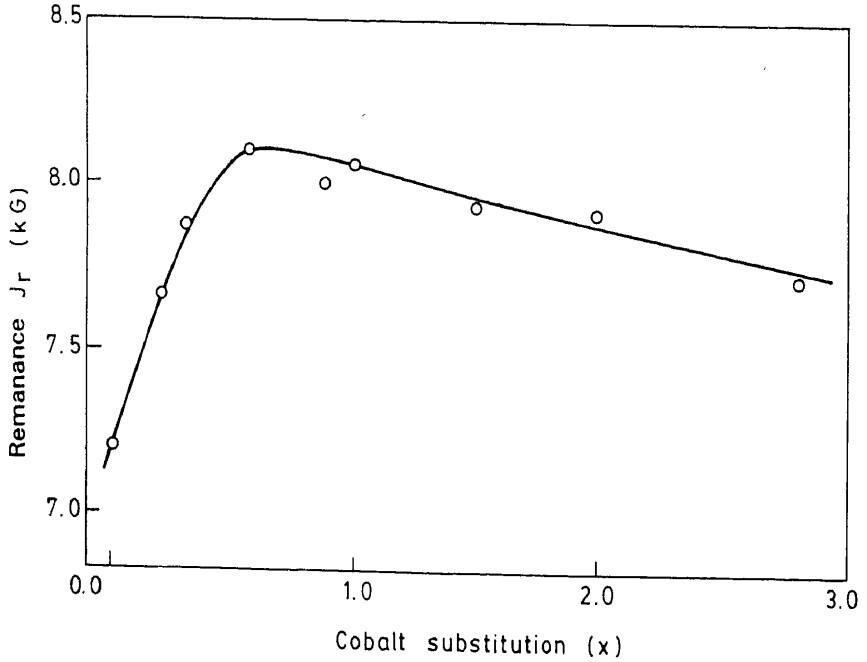

Figure 3. Effect of the cobalt substitution (x) on remanent magnetization J_r in $Pr_{2+\delta}Fe_{14-x}Co_xB$ powders.

by the magnetocrystalline anisotropy H_a, which is lowered by the effectively large Co-substitutions (Buschow 1986). We therefore selected a slightly larger $x \sim 3$ value, as the optimal Co-substitution, to improve the T_c as well and to balance a reasonably

lowered temperature coefficient ($\partial M_s/\partial T$) of the M_s by the improved T_c (at 429°C), suitable for applications as high-energy-density-magnets with steady M_s value over a wide range of temperature of operation at 70°C or lower. This composition ($Pr_{15\cdot5}Fe_{63}Co_{16}B_{5\cdot5}$), which in fact also has a marginally larger excess $\delta = 0{\cdot}71$ Pr, yields the values of $M_s = 150$ emu/g, $H_{ci} = 17$ kOe and $J_r = 7{\cdot}8$ kG at room temperature. The present $H_{ci} = 17$ kOe is significantly lower than the optimal value of 21 kOe, but it is stable and does not decrease further during storing the sample in the ambient atmosphere.

The cobalt substituted $Pr_{2+\delta}Fe_{14-x}Co_xB$, $x \sim 3$, alloys behave to be better stable and corrosion resistant in air. As a result, the $Pr_{15\cdot5}Fe_{63\cdot0}Co_{16\cdot0}B_{5\cdot5}$ alloy powder, which contains a total of 9 wt% excess Pr over the ideal $R_2Fe_{14}B$ composition, minimized the M_s loss at 5% (10% in $Pr_2Fe_{14}B$ and 14% in $Nd_2Fe_{14}B$) in the presumed oxidation during exposure in laboratory air atmosphere. It exhibits a considerably enhanced T_c value from 292°C to 429°C, determined by the thermomagnetogram (figure 4) measured at a constant magnetic field $H = 1$–2 kOe. The Co substitution causes a dramatic increase in T_c in both $Pr_2Fe_{14}B$ and $Nd_2Fe_{14}B$ alloys in similar fashion. In particular, T_c for $Pr_2Fe_{14}B$ ($Nd_2Fe_{14}B$) is 292°C (315°C), while $T_c \sim 730$°C for both $Pr_2Co_{14}B$ and $Nd_2Co_{14}B$.

This powder was used to fabricate into sintered or polymer bonded magnets. The die-upset powder at 40 kOe, measured on as high J_r as 13 kG, i.e. compatible to the value in Nd-based magnets. A special advantage with present magnets, over the Nd-based magnets, is that these can be used also at low temperatures (below 140 K) because these are uniaxial up to 0 K.

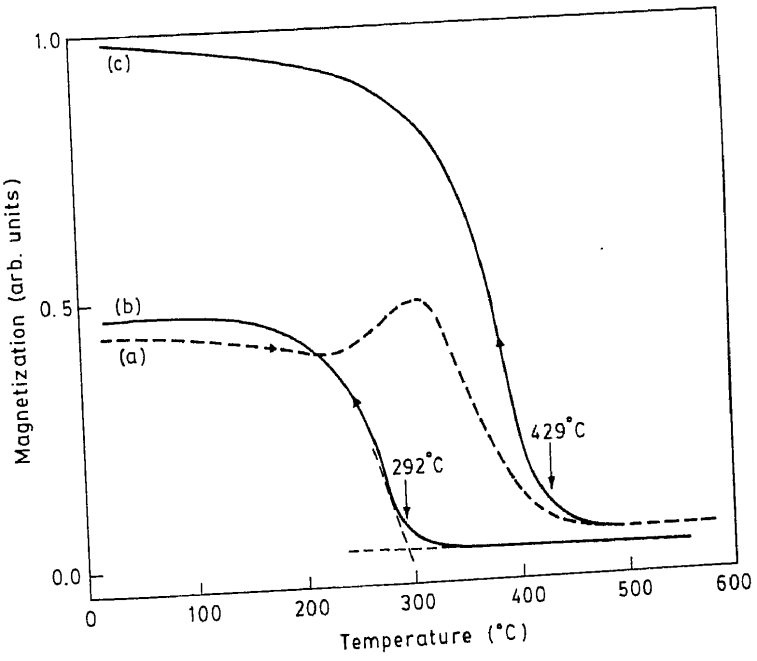

Figure 4. Thermomagnetograms of $Pr_{15\cdot5}Fe_{63\cdot0}Co_{16\cdot0}B_{5\cdot5}$ powder measured at a magnetic field of 2 kOe. Curves (a) and (c) are measured during the heating and cooling, respectively. The T_c is significantly improved from 292°C in curve (b), measured in cooling cycle, to 429°C in curve (a) or (c) on the substitution of the cobalt.

3.2 *Anomalous variation of H_{ci} with tempcrature*

Figure 5 shows the value of H_{ci} plotted as a function of temperature between 4·2 and 600 K for $Pr_{14.5}Fe_{80}B_{5.5}$ alloy. The obtained H_{ci} vs T curve is eventually similar to that portrayed in figure 6 for a Nd-based $Nd_{14.5}Fe_{76.9}Co_{3.1}B_{5.5}$ alloy, which has a $H_{ci} = 17$ kOe value at room temperature. In both the examples, the H_{ci} value monotonically increases with decreasing temperature from $T = T_c$ to 4·2 K. This peculiar variation of H_{ci} with temperature is not well explained by available micromagnetic (Hilzinger and Kronmüller 1977; Kronmüller 1987; Kronmüller *et al* 1987) or pinning (Pinkerton and Fuerst 1990; Kou *et al* 1994) models.

According to the micromagnetic model (Kronmuller *et al* 1987), the value of H_{ci} is written as

$$H_{ci} = \left[\frac{2K_1}{\mu_0 M_s}\right] a_k a_\phi - N_{eff} M_s, \tag{1}$$

where μ_0, a_k, a_ϕ and N_{eff} are the permeability, micromagnetic coefficient, microstructural coefficient, and the local demagnetization factor, respectively. In this model, the second order anisotropy constant K_2 is neglected in comparison to the first order anisotropy constant K_1. The parameters a_k and a_ϕ are the functions of temperature so that they account in the temperature dependence of the H_{ci} value.

In the hard ferromagnetic R–Fe–B alloys, having the microcrystals of $R_2Fe_{14}B$ as the primary phase, a high H_{ci} value usually results in the presence of a R-rich

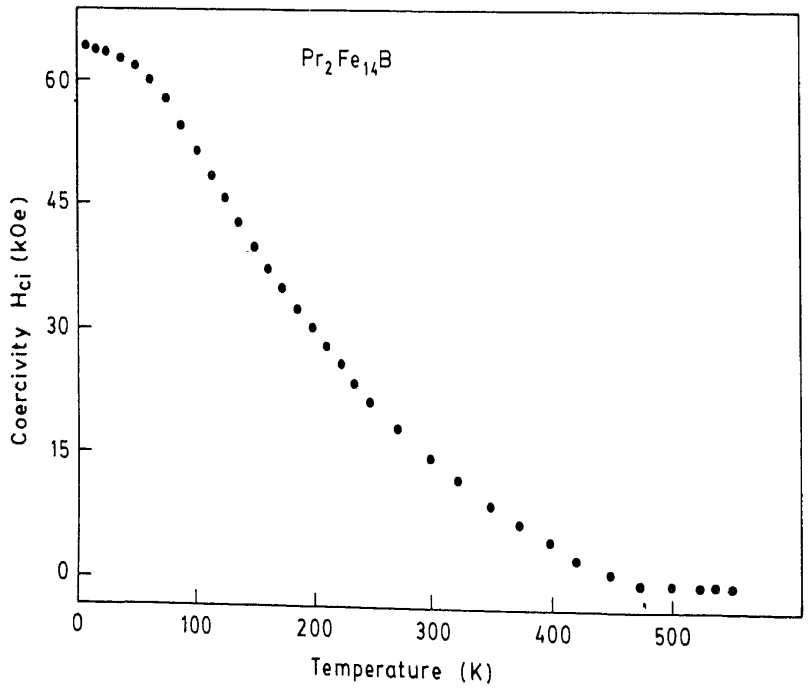

Figure 5. H_{ci} vs T plot for $Pr_{14.5}Fe_{80}B_{5.5}$ powder, which measures a $H_{ci} = 15$ kOe value at room temperature.

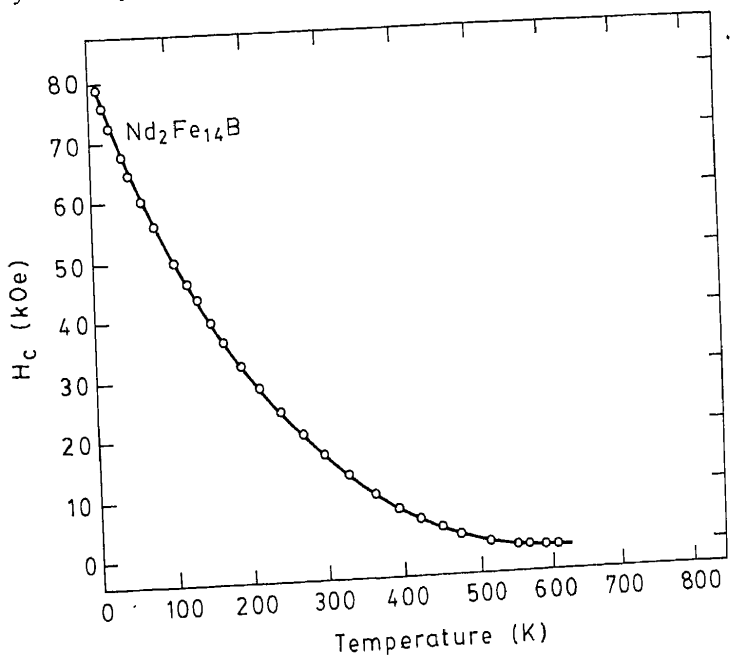

Figure 6. H_{ci} vs T plot for $Nd_{14.5}Fe_{76.9}Co_{3.1}B_{5.5}$ powder, which measures a $H_{ci} = 17$ kOe value at room temperature.

nonmagnetic intergranular phase (Pinkerton and Fuerst 1990). In the compositions, listed in table 1, the excess Pr (or Nd) forms the presumed R-rich intergranular phase with the Fe and/or Co. That coats the ferromagnetic (F) $Pr_2Fe_{14}B$ grains by forming a thin layer, which is believed to be a few nanometer thick (Pinkerton and Fuerst 1990). Although it comprises of the magnetic atoms it surprisingly behaves to be non-magnetic or possibly a diamagnetic (D). It acts as pinning centres to prevent continuous motion of domain walls (F) from grain to grain. In other words, it simply divides mixing of magnetic lines of forces of one grain to other. Therefore, they behave to be isolated single domain particles and consistently result in the enhanced H_{ci} value. The D–F interaction (repulsion) is enhanced by the enhanced magnetic moments in the two phases at low temperatures so that the H_{ci} increases monotonically with decreasing the temperature.

In the absence of this intergranular phase, the domain walls run continuously from grain to grain, forming an extended domain structure, which continue through several grains. If we assume that the $R_2Fe_{14}B$ domain walls are pinned by thin intergranular layers, i.e. $\delta_B > r_0$ (where δ_B is the domain-wall width and r_0 the average half-width of the intergranular layer), H_{ci} is expressed by the relation (Kou *et al* 1994)

$$H_{ci} = (27)^{-1/2}\left[\frac{2\pi r_0 k_1}{\mu_0 \delta_B M_s}\right] - N_{eff} M_s. \tag{2}$$

A comparison of the coefficients in relations (1) and (2) implies $a_k = (27)^{-1/2}\pi r_0/\delta_B$ and $a_\phi = 1$. Moreover, if the $R_2Fe_{14}B$ domain walls are pinned by an extended planar

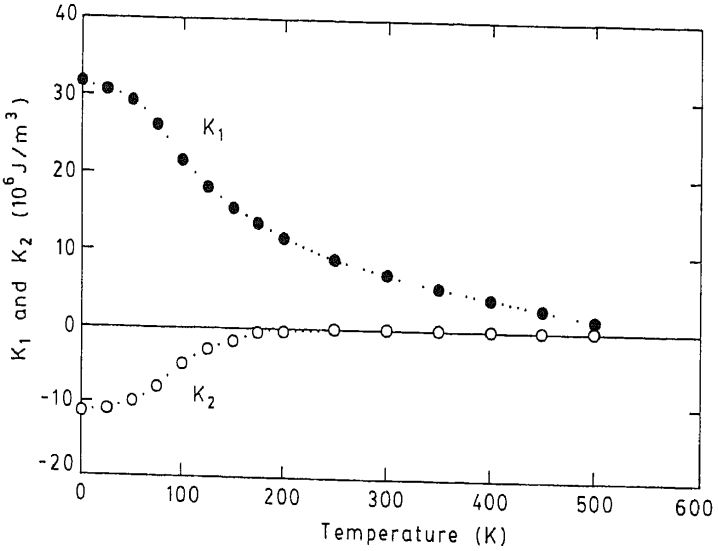

Figure 7. Variation of the anisotropy constants K_1 and K_2 with temperature in $Pr_2Fe_{14}B$ (after Kou *et al* 1994).

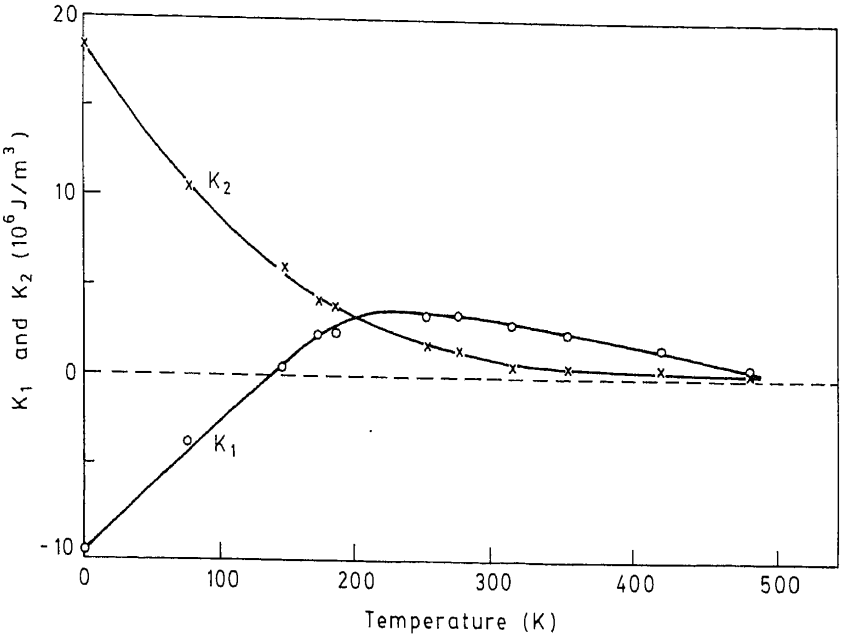

Figure 8. Variation of the anisotropy constants K_1 and K_2 with temperature in $Nd_2Fe_{14}B$ (after Yang *et al* 1985).

intergranular layer, i.e. $\delta_B < r_0$, the above relation becomes (Kronmüller 1987)

$$H_{ci} = \left[\frac{4\delta_B K_1}{3\pi\mu_0 M_s r_0}\right] - N_{eff} M_s, \tag{3}$$

which yields $a_k = 2\delta_B/3\pi r_0$ and $a_\phi = 1$.

Both of the above discussed models only indirectly involve the temperature dependent terms a_k, a_ϕ, K_1 and K_2. The M_s, which is a directly experimentally measured parameter, usually regularly increases in decreasing temperature in the $R_2Fe_{14}B$ ferromagnetic regime, and thus contributes an inversely proportionally decreasing value of H_{ci} as a function of temperature, but it is in an opposite trend to the observed variation of the effective H_{ci} value with temperature. It means that the other terms in the model play a more vital role in governing the viscosity of the high H_{ci} value. It is well established (Buschow 1986; Pinkerton and Fuerst 1990; Kou *et al* 1994) that a high H_{ci} value in $R_2Fe_{14}B$ alloys basically occurs due to the magnetocrystalline anisotropy $H_a = 2K_1/\mu_0 M_s$, which defines the first term in the right hand side in relation (2) or (3). The value of $K_1 \sim 31{\cdot}5\,MJ/m^3$ in $Pr_2Fe_{14}B$ at 0 K (see figure 7) is about 3 times larger than that in $Nd_2Fe_{14}B$ (see figure 8). Of course, in $Nd_2Fe_{14}B$, the value of K_1 is negative and ~ 2 times lower in magnitude than the value of $K_2 \sim 18{\cdot}2\,MJ/m^3$ at 0 K. It indicates that the first order anisotropy constant K_1 in $Pr_2Fe_{14}B$ and the second order anisotropy constant K_2 in $Nd_2Fe_{14}B$ prominently constitute the effective H_{ci} value. Our H_{ci} vs T curve for $Pr_{2+\delta}Fe_{14}B$, with $\delta = 0{\cdot}538$ alloy, in figure 5, thus qualitatively follows the K_1 vs T curve portrayed in figure 7. Likewise, the H_{ci} vs T curve in figure 6 follows the K_2 vs T curve in figure 8 in the Nd-based alloy. Obviously, a realistic model of H_{ci}, which can account in the temperature dependence of it, must include both the anisotropy constants K_1 as well as K_2, and the magnetic viscosity caused by the interactions in the presence of the intergranular phases. Our further work in this series is in progress and the results will be communicated separately.

3.3 *Spin-reorientation transitions*

Our Pr-based alloys, unlike the Nd-based alloys, do not show any spin-reorientation transitions at temperatures below T_c. In the Nd-based alloys, the magnetization decreases with decreasing temperature below a certain value called the spin-reorientation transition temperature T_{SR}. For example, figure 9 shows the thermomagnetograms of a typical sample recorded, between 300 and 4·2 K, at two different magnetic fields of (a and b) 10 kOe and (c) 80 kOe. The total M_s (i.e. the saturation magnetization obtained in the high magnetic field scan of 80 kOe) clearly regularly decreases over low temperatures, effectively below 200°C, with the onset temperature T_{md} at 112 K (determined by the intersection of two straight lines in thermomagnetogram). A physical significance of T_{md} is that it defines a critical temperature below which the total M_s decreases with further decreasing the temperature, led by the spin-reorientations of the magnetic moments of the Fe and Nd atoms in the $Nd_2Fe_{14}B$ lattice. At $T \geqslant T_{md}$, the magnetic moments of both Fe and Nd atoms are collinear with the crystallographic c-axis in $Nd_2Fe_{14}B$ crystal lattice, but they undergo spin-reorientations at T_{SR}, here $T_{SR} \sim T_{md}$, making a resultant angle θ_c with the c-axis, which monotonically increases with further decreasing the temperature up to $T = 0$ K (Lim *et al* 1991).

It is interesting to note that the $Nd_2Fe_{14}B$ single crystals, which do not have any intergranular phase, do not exhibit so pronounced effects of the spin-reorientations on the total M_s. The M_s value in this case regularly increases with the decreasing temperature, showing only a small change in the slope at $T_{SR} \sim 126$ K (Deruelle 1990). In fact, the presumed Nd-rich intergranular phase, which eventually behaves to be non-magnetic (or diamagnetic) compared to the ferromagnetic $Nd_2Fe_{14}B$, modifies

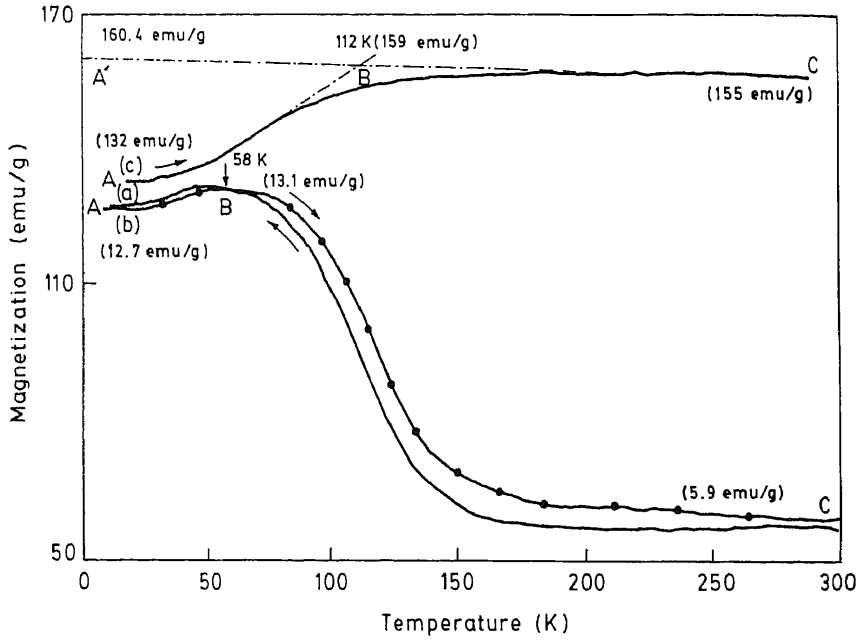

Figure 9. Thermomagnetograms of crystalline $Nd_{15\cdot5}Fe_{63\cdot0}Co_{16\cdot0}B_{5\cdot5}$ powder recorded at (a) 10 kOe, (b) 10 kOe and (c) 80 kOe. Curve (a) is measured in cooling cycle while curves (b) and (c) are measured in the heating cycles. The scale bar on the y-axis applies to curve (c). It is to be divided by a factor of 10 in the other curves.

the exchange interactions (J_{FG}), which are normally neglected (but appear peculiarly important in this particular example), between the ferromagnetic $Nd_2Fe_{14}B$ grains by inhibiting mixing of local magnetic lines of forces over isolated $Nd_2Fe_{14}B$ grains. The modified J_{FG}, on the peculiarly modified $Nd_2Fe_{14}B$ grain-surfaces, eventually led to a modified and pronounced decrease of M_s with decreasing temperature over $T \leqslant T_{SR}$.

Thus the total M_s of this binary (ferromagnetic $R_2Fe_{14}B$ and non-magnetic intergranular phase) magnetic phase material can be written as

$$M_s = (1-x)M_s(F)\cos\theta_c + xM(I), \tag{4}$$

where x is the fractional ratio of the intergranular phase of magnetic moment $M(I)$ and $M_s(F)$ is the magnetic moment of the ferromagnetic $Nd_2Fe_{14}B$ phase, which is modified by a factor of $\cos\theta_c$ in the $T \leqslant T_{md}$ region, by the spin-reorientation transitions.

Relation (4) implies the value of $M(I)$ given by

$$M(I) = -\left[\frac{(1-x)M_s(F)\cos\theta_c - M_s}{x}\right], \tag{5}$$

or

$$M(I) = M_s(F)\cos\theta_c - \left(\frac{\Delta M_{FS}}{x}\right), \tag{6}$$

where $\Delta M_{FS} = M_s(F)\cos\theta_c - M_s$ is the contribution of the intergranular phase to the total magnetization. If we presume $M(I) \sim 0$, our experimental data in figure 9

implies

$$M_s(F)\cos\theta_c = \left(\frac{132}{1-x}\right), \tag{7}$$

and

$$M_s(F) = \left(\frac{160{\cdot}4}{1-x}\right), \tag{8}$$

in emu/g at 4·2 K, obtained by extrapolation of the straight line CB to point A. On dividing relation (7) by relation (8), we get the value of $\cos\theta_c = 1{\cdot}82$, or $\theta_c = 34{\cdot}62°$, which compares well with the resultant tilting angle (of the magnetic moments of the Fe and Nd atoms from the easy axis of the magnetization, i.e. along the crystallographic c-axis in the $P4_2/mnm$ tetragonal $Nd_2Fe_{14}B$ lattice) $\theta_c = 30°$, as reported by magnetization measurements and torque measurements on single $Nd_2Fe_{14}B$ crystals by Tokuhara *et al* (1985).

Incorporating the experimental values of $M_s(F) = 195$ emu/g, for the single crystals (Ram 1995), and $\Delta M_{FS}(= 195\cos\theta_c - 132) = 28{\cdot}47$ emu/g, at 4·2 K, in relation (6), we obtain

$$M(I) = 160{\cdot}47 - \left(\frac{28{\cdot}47}{x}\right), \tag{9}$$

in emu/g at 4·2 K. It predicts a value of $M(I) \sim 0$ (at 4·2 K) at $x \sim 0{\cdot}177$, and a negative value at a reasonably smaller x-value, which is not inadequate in this example.

The magnetic interaction between the two phases depends on (i) the spontaneous magnetization of the ferromagnetic phase, (ii) the field applied to magnetize the specimen, and (iii) the temperature during the measurement. At a given temperature $T \leqslant T_{md}$, where the concerned phase is strongly effective, the interaction indeed varies with applied field and the specimen responds differently at different magnetic fields. At effectively low fields of 10 kOe or lower, it behaves as a soft magnetic material, with a reasonably low H_{ci} value, a low magnetization, and the magnetization peaks up (cf. curves 1 and 2 in figure 9) around 58 K. The shape and size of the peak is reversible with respect to the heating and cooling the sample, but the position of the peak varies with the applied magnetic field, according to the competitive interactions developed between the internal fields in the presence of the applied magnetic field.

4. Conclusions

High coercivity stable magnetic powders (of 1–2 μm particle size) of Pr–Fe–B alloys are developed using (i) a partial substitution (5–16 at%) of cobalt on the Fe sites in the primary $P4_2/mnm$ tetragonal $Pr_2Fe_{14}B$ ferromagnetic phase, and (ii) up to ~ 3·5 at% excess Pr over to the ferromagnetic $Pr_2Fe_{14}B$ composition. The cobalt substitution, together with the excess Pr, maintains a high value of $H_{ci} = 17$ kOe, with reasonably increased Curie temperature from 292°C to 429°C, useful for practical applications of the product as permanent magnets and related devices. The excess Pr with part of the cobalt forms highly corrosion resistant grain boundaries. As a result, the present powders behave to be better stable in the ambient atmosphere.

Acknowledgements

The authors are thankful to Prof. H J Fecht, T U Berlin, Germany, for providing the laboratory facilities for some of the measurements. One of the authors (SH) acknowledges the CSIR, India for the Junior Research Fellowship.

References

Buschow K J H 1986 *Mater. Sci. Rep.* **1** 1
Deruelle M C D, Yamada M, Yamauchi H and Nakagawa Y 1990 *Phys. Rev.* **B42** 10291
Givord D, Tenau P and Viadieu T 1986 *J. Appl. Phys.* **60** 3263
Herbst J F, Croat J J, Pinkerton F E and Yellon Y B 1984 *Phys. Rev.* **B29** 4176
Hilzinger H R and Kronmuller H 1977 *Appl. Phys.* **12** 253
Kou X C, Kronmuller H, Givord D and Rossignol M F 1994 *Phys. Rev.* **B50** 3849
Kronmüller H 1987 *Phys. Status Solidi* **B144** 385
Kronmüller H, Durst K D and Martinek G 1987 *J. Magn. Magn. Mater.* **69** 69
Lim D W, Kato H, Yamada M, Kido G and Nakagawa Y 1991 *Phys. Rev.* **B44** 10014
Nishio H, Yamamoto H, Nagakura M and Uehara M 1990 *IEEE Trans. Magn.* **26** 257
Pinkerton F E and Fuerst C D 1990 *J. Magn. Magn. Mater.* **89** 139
Ram S 1994 *Phys. Rev.* **B49** 9632
Ram S 1995 *IEEE Trans. Magn.* (to be published)
Ram S and Joubert J C 1992 *J. Appl. Phys.* **72** 1164; and *Appl. Phys. Lett.* **61** 613
Ram S, Claude E and Joubert J C 1995 *IEEE Trans. Magn.* **30**
Tokuhara K, Ohtsu Y, Ono F, Yamada O, Sagawa M and Matsuura Y 1985 *Solid State Commun.* **56** 333
Yang F M, Zhao X C, Zhao R W, Yu Z H and Zhang S G 1985 *Proc. 4th int. symp. on magnetic anisotropy and coercivity in rare-earth-transition metal alloys* (ed.) K Strnat (Dayton: Dayton Univ. Press) p. 529